PAPER

Check for updates

Augmented interaction of multivalent arginine coated gold nanoclusters with lipid membranes and cells†

Estelle Porret,[a] Jean-Baptiste Fleury, [b] Lucie Sancey, [a] Mylène Pezet, [a] Jean-Luc Coll [a] *[a] and Xavier Le Guével [a] *[a]

A library of ultra-small red photoluminescent gold nanoclusters (Au NCs) were synthesized with an increasing amount of positive charges provided by the addition of mono-, di- or trivalent-glutathione modified arginine peptides. We then studied how the arginine content impacted on the interaction of Au NCs with negatively charged artificial lipid bilayers and cell membranes. Results indicated that increasing the arginine content enhanced Au NCs' adsorption on lipid bilayers and on cell membranes followed by an increased cellular uptake in melanoma cells (COLO 829). Surprisingly, the presence of up to 40% serum for highly positively charged Au NCs did not hinder their interaction with lipid bilayers that contain glycolipids, suggesting a reduced opsonization of these Au NCs. In addition, these Au NCs are usually not toxic, except those with the highest arginine contents. Thus, controlled grafting of arginine peptides onto Au NCs is an elegant strategy to improve their binding and internalization by tumor cells while still keeping their anti-fouling properties.

Metal nanoparticles (NPs) are widely used for biological applications such as bioimaging, drug delivery and photo/radio-therapy.[1–3] To design efficient NPs, it is important to better understand how they interact with the microenvironment, and in particular with cell membranes[4] and blood components.[5] The physico-chemical features of the NPs such as size, electrical charge, composition, and shape directly impact on their biophysical properties such as their colloidal stability and bioavailability in physiological environments.[6] While positively charged molecules usually penetrate cell membranes without disrupting the lipid bilayer,[7,8] positively charged NPs,[9,10] might go through the membranes by creating holes,[10,11] that may induce a certain toxicity. Furthermore, the correlation between NP's interaction with the cells, their intracellular accumulation and their cytotoxicity strongly depends on the cell type, the experimental conditions (culture medium with or without serum, incubation time, concentrations…) and the physico-chemical properties of the NPs (size, shape, hydrophobicity and surface charge…).[12–14]

Ultra-small gold NPs with core size smaller than 3 nm, named gold nanoclusters (Au NCs), are intermediary species

between small molecules and NPs. Due to their photo-luminescent (PL) property,[15] Au NCs do not need further labelling with a fluorescent dye to track them in the cells.[16] This allows us to study directly how modification of their surface properties influence their interaction with biological membranes. Due to their ultra-small size, Au NCs exhibit a high surface reactivity and high diffusion which will drive their interaction with biological barriers. For instance, it was shown a significant impact of surface hydrophobicity for Au NCs to reduce protein adsorption and to improve intracellular accumulation.[17]

Glutathione (SG), a zwitterionic tripeptide present in the cytosol of the cells to maintain their intracellular redox homeostasis,[18] has been widely used as a ligand for the synthesis of Au NCs.[19,20] In addition to being biocompatible, SG generates an electrostatic hindrance that moderate the non-specific binding of Au NCs with surrounding proteins[21] but also with the cell-membranes.[22,23] It is thus relevant to develop new Au NCs with improved binding to the cell membranes and efficient internalization. Peptides containing arginine amino acids have often been used as cell-penetrating peptides due to the interaction of the positive guanidinium moiety with the negatively charged plasma membrane at physiological pH.[24] For this reason, we used glutathione modified with one to three arginines (SG-XArg, X = 1, 2 or 3) as new ligands to stabilize Au NCs using a well-establish method to synthesize monodisperse Au NCs (Scheme 1). We could obtain five different Au NCs with a fine control of their size and their surface chemistry. The

[a]Cancer Targets & Experimental Therapeutics, Institute for Advanced Biosciences (IAB), University of Grenoble Alpes (UGA)/INSERM-U1209/CNRS-UMR 5309, Grenoble, France. E-mail: xavier.le-guevel@univ-grenoble-alpes.fr

[b]Experimental Physics and Center for Biophysics, Saarland University, D-66123 Saarbrücken, Germany

† Electronic supplementary information (ESI) available. See DOI: 10.1039/c9ra10047d
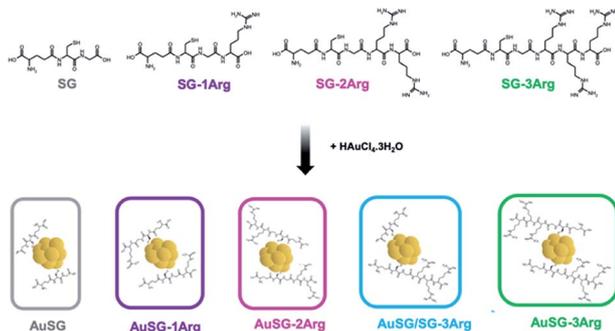
Scheme 1 Synthesis route of Au NCs with SG and SG-*X*Arg peptides (*X* = 1, 2, 3).

extended optical and physico-chemical characterizations of these Au NCs have been recently reported elsewhere by our team.[25]

In this study, we are particularly interested to investigate the behaviour of these positively charged Au NCs with biological barriers in presence of serum using artificial phospholipid models integrated in microfluidic devices[14,17,26] and then with living cells. We demonstrated how increasing slightly the positive charges on Au NC surface can lead to strong interaction with artificial lipid bilayers and cell membrane in the presence of serum. These assays are in favor of a weak opsonization of these ultra-small particles. A precise tuning of the amount of arginine on Au NC surface enables their rapid binding and strong internalization in melanoma cell lines with low toxicity.

1. Methods

1.1 Materials

Arginine modified-glutathione peptides (SG-1Arg = $C_{16}H_{29}N_7O_7$-$S(CF_3COO^-)$; SG-2Arg = $C_{22}H_{40}N_{11}O_8S$ $(CF_3COO^-)_2$; SG-3Arg = $C_{28}H_{53}N_{15}O_9S(CF_3COO^-)_3$ with 10% of H_2O and purity $\geq$ 95%) were purchased from GenScript (USA). Gold(III) chloride trihydrate ($HAuCl_4 \cdot 3H_2O$, reagent grade), reduced L-glutathione ($\geq$98%), sodium borohydride ($NaBH_4$), isopropyl alcohol (IPA, 99%) were purchased from Sigma-Aldrich (France). Sodium hydroxide (NaOH, 98%) and hydrochloric acid (HCl, 35–37%), were purchased from Laurylab and VWR Chemicals BAH. Formvar carbon grids were purchased from Agar scientific. Phosphate buffer (PBS, 10 mM) and cell culture medium (DMEM, Dulbecco's Modified Eagle's medium) were purchased from Gibco (Thermo-fisher, France). All products were used as received without further purification. Water was purified using a Millipore Milli-Q system (Millipore, France) for all experiments.

1.2 Synthesis of Au NCs

Au NCs stabilized by SG or SG-*X*Arg (*X* = 1, 2 or 3) were prepared by wet chemistry as described in our previous study[25] and reported in the ESI† (Section 1). Au NCs were dissolved in PBS (10 mM, pH 7.4) at 4 mgAu mL^{-1} and filtered through a 0.2 μm syringe filter (PTFE membrane).

1.3 Au NCs characterization

Fluorescence spectra of Au NCs solutions were recorded on a Fluoromax-4 spectrometer (HERIBA Scientific) between 470 and 870 nm ($\lambda_{exc.}$ = 450 nm).

High-resolution transmission electron microscopy (HRTEM) images were measured on a JEOL 2010 LaB6 microscope operating at 200 kV with a 0.19 nm point-to-point resolution, after the deposition of the Au NCs (10 μL, 4 mgAu mL^{-1}) on a formvar carbon grid. The images were analyzed with ImageJ software.

Zeta potential measurements of Au NCs solutions were performed in triplicate at 25 °C on a Zetasizer (Malvern). The refractive index (n), the viscosity (η) and the dielectric constant (ε) of the solvent were obtained as described below for PBS: n = 1.34, η = 1.1 mPa s and ε = 79; DMEM: n = 1.33, η = 1.09 mPa s and ε = 78, and DMEMc *i.e.* DMEM supplemented with 10% of heat-inactivated FBS: n = 1.33, η = 1.14 mPa s and ε = 77.6.

1.4 Fabrication of the free-standing phospholipid bilayer

A microfluidic device was set up using Sylgard 184 (Dow Corning) and sealed with a glass microscope slide using standard soft-lithographic protocols.[27] The central part of the device consists of two parallel microchannels, which are connected by a rectangular opening. Liquid flows were controlled using syringe pumps, and the entire process was monitored by optical microscopy (Zeiss Axio Observer Z1). For simultaneous electrophysiological measurements (EPC 10 USB – Heka Electronics), Ag/AgCl electrodes were inserted into the microfluidic device. Bilayers were formed using a variant of the droplet-interface bilayer technique (DiB). In the first step, the device was filled with a squalene oil (Sigma-Aldrich, Germany) and a mixture of 1,2-dioleoyl-*sn*-glycero-3-phosphocholine (DOPC from Avanti Polar Lipids),1,2-dioleoyl-*sn*-glycero-3-phospho-L-serine (DOPS from Avanti Polar Lipids) and a glycolipid (GM1 from Avanti Polar Lipids). DOPC is a neutral lipid and it is the most present lipid in mammalian cell membranes. DOPS is a negatively charged lipid also naturally present in present in mammalian cell membranes but at lower molar ratio (~10%). GM1 (monosialotetrahexosylganglioside) is a ganglioside that is present on cell surfaces, they are predominant in the nervous system where they constitute ~6% of all phospholipids.[28] In the second step, two water fingers were slowly injected into the microchannels. Within a few seconds, the water–oil interface of each finger was covered with a phospholipid monolayer. When the two lipid monolayers are brought into contact at the rectangular opening, they formed a free-standing DOPC/DOPS/GM1 bilayer within seconds. After the formation of a stable phospholipid bilayer, the aqueous solution on each side of the bilayer could be exchanged to solution without breaking the bilayer by flushing aqueous solution through the straight channels.[29]

1.5 Capacitance measurement of the lipid bilayer system

The formation of a DOPC/DOPS/GM1 bilayer was confirmed by electrophysiological measurements, which give the capacitance of the bilayer. We normalize the capacitance values according to

the membrane area ($\sim$110 μm radius for the spherical membrane) to express results in specific capacitance C_s values, with $C_s \approx 3.9$ mF m^{-2} for the pure DOPC bilayer. Using the electrical replacement circuit of a plate capacitor, the DOPC bilayer thickness can be calculated as $d \approx \varepsilon_0\varepsilon_L/C_s \approx 4$ nm, with the vacuum permittivity $\varepsilon_0 \approx 8.85 \times 10^{-12}$ F m^{-1} and $\varepsilon_L \sim \varepsilon_{oil} \sim 2.2 \times 10^{-12}$ F m^{-1}. Thus, the specific capacitance of the pure bilayer should decrease if NCs are inserted fully or partially into the membrane. Each type of Au NCs (100 μgAu mL^{-1}) dispersed in PBS at increasing serum concentrations (0, 5, 10, 20, 30, and 50%) was injected into the two compartments and left to sit for 1 hour before measurement. Exceeding Au NCs concentrations of 100 μgAu mL^{-1} led to a rupture of the formed DOPC bilayer. All experiments were repeated at least 8 times to obtain statistically relevant data. To distinguish whether the Au NCs were only adsorbed on the bilayer surface or truly inserted into the bilayer, new capacitance measurements were conducted after strongly flushing the compartments with a PBS buffer solution through the channels. If the specific capacitance did not reach the initial value of a pure DOPC bilayer, we could safely assume that Au NCs were inserted partially or fully in the membrane.[17]

1.6 Cell culture

Human COLO 829 cells derived from human skin melanoma were purchased from the American Type Culture Collection (ATCC® CRL1974™) and cultured at 37 °C and 5% CO$_2$ in complete medium (DMEMc), i.e. DMEM supplemented with 10% of heat-inactivated FBS (Fetal Bovine Serum, Thermo Fisher Scientific, France), 1% penicillin–streptomycin, and 2 mM L-glutamine (Sigma-Aldrich).

1.7 Flow cytometry experiments

COLO 829 cells were either seeded in a 6-well plate (250 000 cells per well in 5 mL of DMEMc) 1 day before the experiment or used as cell suspension (500 000 cells per Eppendorf). The Au NCs were added at 37 °C or 4 °C to the cells in DMEMc or DMEM at different concentrations (10, 25 or 100 μgAu mL^{-1}) for the indicated times (5, 15, 30, 45 min or 1 h). In both cases, the cells were centrifuged before being resuspended in PBS and analyzed.

Control samples without Au NCs were also included. Each experiment was repeated three times independently.

Measurements were performed on BD-LSR II (BD Biosciences, USA) using the 405 nm laser for excitation and the signal was collected at 780/60 nm after a long-pass 750 nm filter. The results are expressed as percentage of gated cells which internalized the Au NCs based on the control experiments (cells incubated without Au NCs).

1.8 Fluorescent microscopy experiments

COLO 829 cells were seeded in 4-well Nunc Lab-Tek I chambers (100 000 cells per well in 500 μL of DMEMc) 1 day before the experiment. The medium was then changed, and cells were incubated with Hoechst 33342 (1 μM) to stain the nucleus for 30 min at 37 °C. The cells were washed three times with PBS before a 30 min incubation at 37 °C with Au NCs at 25 or 100

μgAu mL^{-1} in DMEMc without phenol red. Cells were washed again three times before being imaged on a 37 °C pre-warmed chamber with CO$_2$. Control samples without Au NCs were also imaged.

Fluorescence microscopy was performed on a Carl Zeiss LSM710 laser confocal microscope, using a plan-Apochromat 60x NA 1.4 oil-immersion objective and an APD detector ($\lambda_{exc.}$ = 405 nm, $\lambda_{em.}$ = 736 nm long pass filter, 380 nm resolution).

Analyses were performed with the ICY software (Institut Pasteur Bioimage Analysis).[30]

1.9 Cytotoxicity experiments

COLO 829 cells were seeded in a 96-well plate (1000 cells per well in 100 μL of DMEMc) 1 day before the experiment. Au NCs were diluted in DMEMc to reach the following final concentrations: 10, 50, 100, 250, 750 and 1000 μgAu mL^{-1} and added to the cells. Cell viability was evaluated 24 h, 48 h or 72 h after Au NCs incubations. The 24 h incubation time experiment was performed in triplicate, as well as the 48 h and 72 h incubation time experiments for 50 or 250 μgAu mL^{-1}. For positive and negative controls, cells with or without 1 μM staurosporine treatment (cell-death inducer) were also prepared. In order to verify the absence of artefact due to the absorption of the Au NCs, wells with only Au NCs in DMEMc were also prepared. Then 20 μL of MTS reagent (Cell-Titer 96, Promega) was added to each well and further incubated at 37 °C for 2 h. The cell density was then determined by the absorbance at 486 nm using a microplate spectrophotometer (Fluostar Omega BM6 LAB-TECH). The percentages of cell viability were compared using the non-parametric Kruskal–Wallis test. All analyses were performed using GraphPad Prism software. Statistical significance was defined as p values < 0.05.

2. Results

We synthesized five types Au NCs with different charges stabilized by the following ligands: SG, SG-1Arg, SG-2Arg or SG-3Arg or with a mix of SG/SG-3Arg (with a ligand ratio of 25/75%).

2.1 Au NCs characterization

The five different Au NCs showed broad photoluminescent (PL) emissions between 570 and 860 nm with a maximum at $\lambda_{em.} \sim$ 670 nm (Fig. 1A). The PL intensity increased and is red-shifted of $\sim$20 nm with the amount of arginine on Au NC surface until to reach a maximum at 75% of AuSG-3Arg and then strongly decreased for Au NC containing a full coverage of SG-3Arg ligand. In this case, the fluorescence enhancement has been mainly attributed to a rigidification of the ligand shell around the gold core reducing the non-radiative losses.[25]

HRTEM pictures (Fig. 1B) showed metal core size below 3 nm for all samples except for AuSG-3Arg which contained larger particles (>10 nm, NPs). Spectroscopic measurements by XPS and NMR, elemental analyses and mass spectrometry confirmed the relatively high monodispersity of these Au NCs (except for AuSG-3Arg) with the organic shell corresponding to $\sim$50 wt% of each particle.[25]
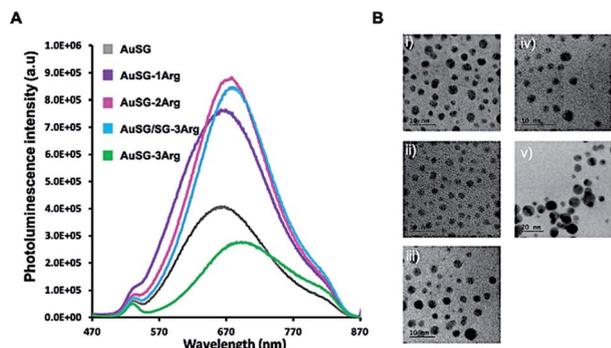
Paper

Fig. 1 (A) PL spectra of diluted Au NCs in water (0.04 mgAu mL^{-1}, pH 7.0) at the same optical density (0.04 OD) between 470 and 870 nm ($\lambda_{exc.}$ = 450 nm). (B) HRTEM of Au NCs stabilized by (i) SG, (ii) SG-1Arg, (iii) SG-2Arg, (iv) SG/SG-3Arg (25/75) (scale bar 10 nm), and (v) SG-3Arg (scale bar 20 nm).
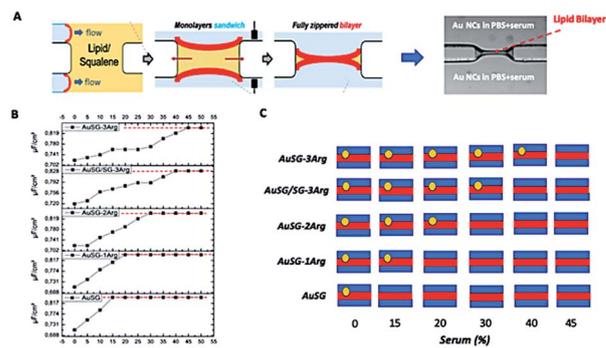

Fig. 2 (A) Scheme of the fabrication of DOPC lipid membrane in a microfluidic device and observed by optical microscopy. (B) Capacitance measurements C_s of the five types of Au NCs as a function of the serum concentration with a 12% DOPS lipid membrane. The red dash line corresponds to the initial specific capacitance, *i.e.* the specific capacitance of a bilayer without Au NCs. (C) Summary of Au NC interactions with the DOPC membrane as a function of the ligand protecting the Au NC surface and the serum content in the compartment.

The zeta potential of the Au NCs in PBS or in DMEM shifted from negative (for AuSG and AuSG-1Arg) to positive (for AuSG-2Arg, AuSG/SG-3Arg and AuSG-3Arg) at pH 7.4 when increasing the amount of arginine (Table 1). Interestingly, all types of Au NCs exhibited similar global negative zeta potentials in DMEMc, *i.e.* in the presence of 10% heat-inactivated bovine serum, probably due to their interaction with proteins. However, we should be careful on this last interpretation as zeta potential measurements of such ultrasmall nanoparticles correspond to an average value of all charged materials in solution including free proteins. After 48 h of storage in PBS at room temperature and pH 4 the PL of each Au NCs remains almost constant while it slightly decreased at pH 5, especially for the AuSG-2Arg and AuSG/SG-3Arg which showed a two-fold decrease. However, the PL intensities of AuSG-2Arg and AuSG/SG-3Arg were still higher than that of AuSG-3Arg (Fig. S1†).

2.2 Au NCs' interaction with lipid bilayers

The interaction of the Au NCs with a model membrane was investigated using a DOPC/DOPS lipid bilayer in a microfluidic device (Fig. 2A). The negative electrostatic charge of the membrane is controlled by the molar concentration of negatively charged DOPS lipids. The different Au NCs functionalized with arginine were diluted at a final concentration of 100 μgAu mL^{-1} in serum (from 0% to 50% v/v in PBS) and injected into the two sides of the lipid bilayers. We let the system equilibrate

for 1 hour and rinsed both sides of the bilayer to remove all unbound Au NCs. It should be noticed that the insertion of Au NCs into the bilayer leads to a decrease of specific capacitance C_s (see Methods 1.4 and 1.5). No Au NCs were observed to go across the lipid bilayer excluding passive particle translocation.

As shown in Fig. 2B and S2,† all Au NCs were detected in the lipid bilayer in the absence of serum. The specific capacitance C_s of the pure DOPC bilayer (membrane with neutral charge) was not affected by the serum content. There was a clear delay to reach the threshold C_s of the pure layer (red line) when increasing the serum concentration from 0 to 50% and this effect was more pronounced with the amount of arginine stabilizing the AuNCs: AuSG > AuSG-1Arg > AuSG-2Arg > AuSG/SG-3Arg ∼ AuSG3-Arg (see Fig. 2B, C and S2†).

This effect was also amplified when increasing the amount of negatively charged lipids present in the lipid bilayer including with GM1 as charged glycolipid[31] (Fig. 3A). It suggests that the more Au NCs are positively charged, the more they interact with charged membranes (for example, up at 40% serum for the most positively charged Au NCs). Thus, the insertion of a type of NC into a bilayer seems to be mainly determined by the electrostatic interaction between the lipid bilayer membrane and the NCs. We incorporated GM1, a glycolipid present at elevated

Table 1 Zeta potential measurements performed on diluted Au NCs solutions (0.04 mgAu mL^{-1}) at pH 7.4 in different media (PBS, DMEM and DMEMc). Results are expressed as mean ± standard deviation (n = 3)

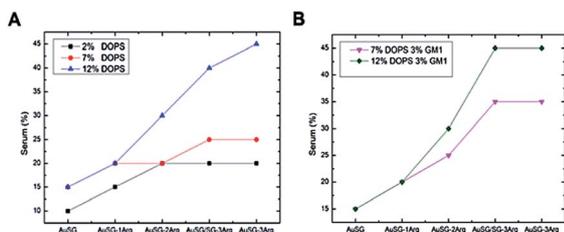| NCs	Zeta potential in PBS (pH 7.4, mV)	Zeta potential in DMEM (pH 7.4, mV)	Zeta potential in DMEMc (pH 7.4, mV)
AuSG	−17.2 ± 0.3	−19.4 ± 0.3	−11.9 ± 0.4
AuSG-1Arg	−9.1 ± 0.8	−6.4 ± 1.6	−10.5 ± 0.7
AuSG-2Arg	4.3 ± 0.6	10.0 ± 0.2	−10.3 ± 1.0
AuSG/SG-3Arg	6.6 ± 1.0	9.4 ± 1.1	−10.1 ± 1.4
AuSG-3Arg	12.0 ± 063	17.5 ± 0.3	−8.0 ± 0.9

Fig. 3 Summary of Au NC interactions with the lipid membrane as a function of the type of NC, the amount of charged lipids (PS) and the serum content (A) and in present of the glycolipid GM1 (B). 12% DOPS corresponds to the average standard concentration of negatively charged lipids in a mammalian cell membrane.

concentrations in many cell membranes,[32] within the phospholipid bilayer. Results depicted in Fig. 3B, indicate an increase of Au NCs uptake with 3% of GM1 for the positively charged Au NCs.

2.3 Au NCs' interaction with cells

2.3.1 Impact of the Au NCs charges, concentration and medium. Adherent COLO 829 cells were incubated with the Au NCs (10, 25 or 50 µgAu mL^{-1}) in DMEM and DMEMc for 30 minutes at 37 °C, washed and analyzed by flow cytometry after trypsinization. The percentage of cells labeled by Au NCs increased with the amount of arginine (Fig. 4). Even with the highest concentrations of AuSG and AuSG-1Arg, the percentage remained similar to the control, *i.e.* almost 0%. In contrast, AuSG-2Arg and AuSG/SG-3Arg were already able to label 70% of the cells and 100% for AuSG-3Arg at the lowest tested concentration (10 µgAu mL^{-1}). These interactions were dose

dependent for AuSG-2Arg and AuSG/SG-3Arg from 10 to 50 µgAu mL^{-1}. A similar trend was also observed in DMEMc, indicating that the presence of serum did not impact on their interaction with the cells.

We observed also the same results with cells in suspensions instead of lying on the bottom of the well plate (Fig. S3†). However, the dose dependence threshold between 10 and 25 µgAu mL^{-1} for AuSG-2Arg and AuSG/SG-3Arg, was more pronounced. We thus kept the cells incubated in suspension with 25 µgAu mL^{-1} of Au NCs as a standard protocol for the next experiments.

2.3.2 Impact of the incubation time. COLO 829 were incubated at 37 °C for 5, 15, 30, 45 or 60 min with the Au NCs to study their binding kinetics in DMEM (Fig. 5A) and DMEMc (Fig. S4A†). While longer incubation time did not enhance the cell binding of AuSG and AuSG-1Arg, we surprisingly observed a decrease of the percentage of labeled-cells with AuSG-2Arg and AuSG/SG-3Arg with the incubation time. This trend was obtained when the cells were kept at 37 °C but not at 4 °C, especially in DMEM. The percentage of positive cells was divided by 2 after 45 min in the presence of AuSG-2Arg. This decrease of the mean fluorescence intensity (see also Fig. S5†) suggests either that AuSG-2Arg is rapidly released from the cells or degraded with a subsequent loss of PL.

2.3.3 Impact of the temperature. We reproduced the previous experiment at 4 °C in DMEM (Fig. 5B) and DMEMc (Fig. S4B†) to inhibit the energy-dependent internalization. Cellular interactions were still undetectable for AuSG and AuSG-1Arg. Interestingly, 100% of the gated cells were immediately labeled with either AuSG-2Arg, AuSG/SG-3Arg or AuSG-3Arg and this labeling remained constant over time except fo AuSG-2Arg which seemed to be re-exported rapidly by the cells at 37 °C.

2.3.4 Intracellular localization of Au NCs. The presence of Au NCs (0.25 µgAu mL^{-1}) in COLO 829 cells after 30 min of incubation in DMEMc was followed by confocal microscopy. To avoid potential artifacts, cells were imaged alive on a 37 °C prewarmed chamber with CO$_2$. The results were in agreement with the previous ones obtained by flow cytometry (Fig. 6). The fluorescence intensity of cells incubated with AuSG or AuSG-1Arg was indistinguishable from the background of untreated
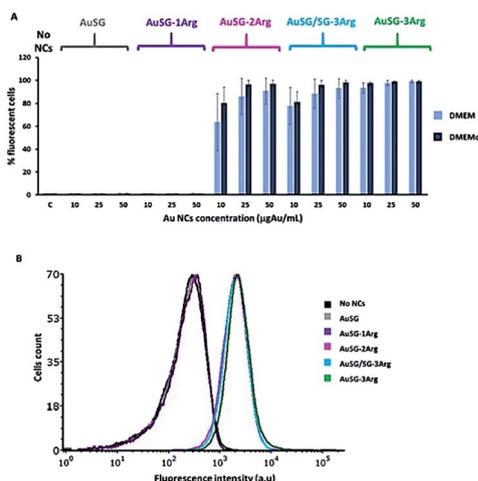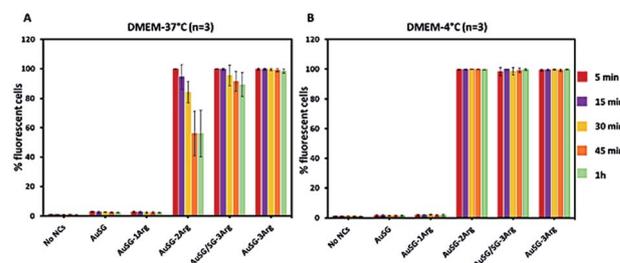

Fig. 4 (A) Fluorescence labeling of adherent COLO 829 cells by the different Au NCs is arginine and dose dependent. Flow cytometry measurements were performed with increasing concentrations of Au NCs (10, 25 and 50 µgAu mL^{-1}) in DMEM or DMEMc at 37 °C for 30 min. Results are expressed as mean ± standard deviation (n = 3, number of cells per gate = 10 000 cells). (B) Representation of the variation of mean fluorescence intensity after incubation of COLO 829 cells with the different Au NCs (50 µgAu mL^{-1}, 30 min, 37 °C, DMEM).

Fig. 5 Flow cytometry measurements of COLO 828 cells in suspension with the five different Au NCs. Cells were incubated in DMEM at 25 µgAu mL^{-1} for 5, 15, 30, 45 and 60 min to evaluate the kinetics of particle interactions with the cells at (A) 37 °C or (B) 4 °C. Results are represented as mean ± standard deviation (n = 3, number of cells per gate = 10 000 cells).
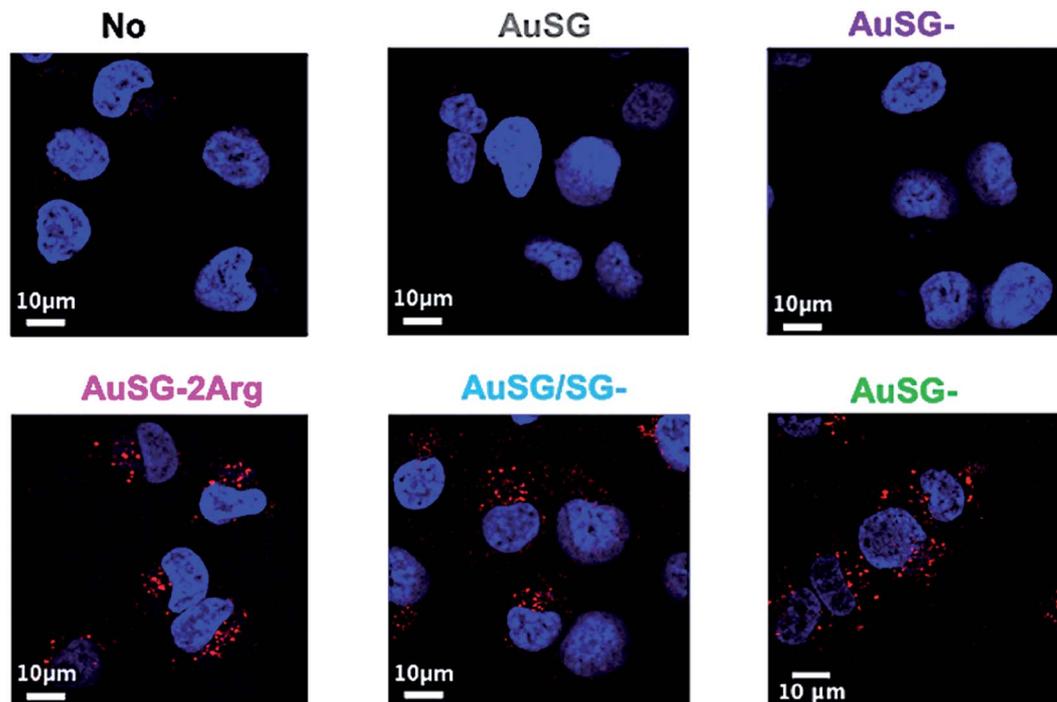
Fig. 6 Au NCs fluorescence (red) merged with Hoechst 33342 staining of the nucleus (blue) of COLO 829 cells incubated without Au NCs or with 25 μgAu mL^{-1} of AuSG, AuSG-1Arg, AuSG-2Arg, AuSG/SG-3Arg and AuSG-3Arg.

cells (autofluorescence), while we could clearly distinguish the presence of fluorescent dots within the cells incubated with AuSG-2Arg, AuSG/SG-3Arg or AuSG-3Arg. These Au NCs were never detected in the nucleus of the cells.

2.4 Cytotoxicity assays

We evaluated the viability of melanoma COLO 829 cells (Fig. 7) and human fibroblasts MRC5 (Fig. S6†) incubated with a wide range of concentrations of Au NCs (50, 100, 250, 500, 750 and 1000 μgAu mL^{-1}) for 24 h. The results illustrated in Fig. 7 showed low toxicity in presence of AuSG or AuSG-1Arg, with

more than 80% viability even at the highest concentration. AuSG-2Arg and AuSG/SG-3Arg showed reduced toxicity with more than 70% of the cells surviving to concentrations ≤250 μgAu mL^{-1} and less than 65% when the dose was reaching 500 μgAu mL^{-1}. In contrast with AuSG-3Arg less than 40% of the cells survived to the concentrations ≥100 μgAu mL^{-1}. The concentration values inhibiting cell growth by 50% (IC$_{50}$) were: AuSG-2Arg (550 μgAu mL^{-1}) < AuSG/SG-3Arg (438 μgAu mL^{-1}) < AuSG-3Arg (70 μgAu mL^{-1}).

Time dependence toxicity was also evaluated (Fig. S7†). The doubling time of the cells were not affected with AuSG, AuSG-1Arg, AuSG-2Arg and AuSG/SG-3Arg at 50 or 250 μgAu mL^{-1} for 72 h. In contrast, we observed that the AuSG-3Arg at 50 μgAu mL^{-1} lower the cell growth and inhibit them at 250 μgAu mL^{-1} due to a very strong an immediate toxicity.

3. Discussion

We investigated how increasing the amount of arginine on Au NC surface influenced their interactions with artificial charged phospholipid membranes and with cancer cells in the presence of serum. For this purpose, we selected Au NCs stabilized by glutathione (SG) and glutathione modified with 1, 2 or 3 arginines (SG-1Arg, SG-2Arg, SG-3Arg) ligands which enabled to finely control the surface charge with a direct correlation between the positive charge of Au NCs and the amount of arginine.

Several studies have reported the higher adsorption of positively charged NPs on cell membranes by electrostatic interactions compared to neutral or negatively charged NPs
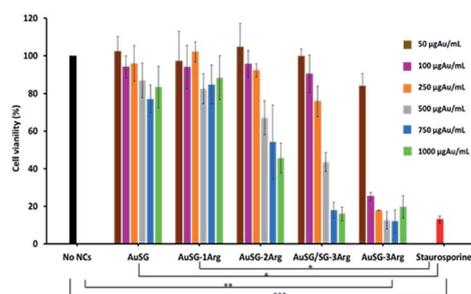

Fig. 7 Evaluation of the cell viability in presence of increasing amounts of Au NCs. COLO 829 cells were incubated with the five Au NCs from 50, 100, 250, 500, 750 to 1000 μgAu mL^{-1} for 24 h in DMEMc. Staurosporine was used as a positive control of cell death. Cell viability was measured using a MTS assay. Results are represented as mean ± standard error of 3 independent experiments (***$p < 0.001$, **$p < 0.01$ and *$p < 0.05$).

leading to higher cellular uptake.[9,11] Our results by flow cytometry were consistent with these studies confirming a direct correlation between an increase of Au NCs-cells interactions and the amount of arginine on Au NC surface in PBS or in DMEM with or without serum (Fig. 4 and S3†) in agreement with previous studies.[13,22,33]

The modification of Au NC surface charges in presence of serum are usually attributed to the non-specific adsorption of the different serum components like proteins forming a corona layer. The nature and the stability of this corona layer are highly dependent on NP size and shape, surface charge and on the specific organization of the ligand shell. Due to the ultra-small core-size of the Au NCs (below 3 nm), the number of serum components interacting with Au NCs should be limited. In our case, the adsorption of the Au NCs onto an artificial lipid bilayer is driven by electrostatic interaction (Fig. 2C and 3). This experiment clearly showed that the insertion of Au NCs into the lipid bilayer was proportional to the number of arginine moieties when the serum content in solution and the negative charges of the model membrane increased. These results also confirmed the reduced opsonization of Au NCs in high serum content up to 40% for the most positively charged Au NCs and indicate the strong anti-fouling properties of such particles due to their ultra-small size. This antifouling effect allows the Au NCs to keep their initial electro-positivity no matter the presence of serum, and thus to bind the negatively charged membranes proportionally to their charge.

Another explanation to the reduced opsonization of these Au NCs could be related to the composition and organization of the ligand shell on the Au NCs as a function of the number of arginine. Indeed, the first arginine has a spatial proximity with the SG and form a rigid inner layer whereas the second and third arginine would rather form a flexible and accessible outer layer.[25] The local attraction between the arginine and the membrane could overcome the global electrostatic repulsion and makes possible the adsorption of AuSG-2Arg, AuSG/SG-3Arg and AuSG-3Arg onto negatively charged membranes. On the contrary, for AuSG-1Arg all the arginines might be hidden by either the SG or after the adsorption of serum components which would reduce the probability of interaction with cell membranes. This hypothesis is in agreement with previous reports highlighting the role of ligand composition and order in cell-membrane penetration.[7,33] For example, A. Verma et al. have demonstrated that negatively charged Au NPs (~6 nm core size) stabilized by a well-organized shell of anionic and hydrophobic ligands were able to cross the negatively charged cell membrane. On the contrary, when the ligand shell was disorganized the Au NPs were not able anymore to penetrate the cell membrane.

To investigate the mechanism by which these particles entered the cells, we performed kinetics experiments at 4 °C by flow cytometry (Fig. 5 and S4†). We observed that AuSG-2Arg, AuSG/SG-3Arg and AuSG-3Arg interacted quickly with the cell (by adsorption on the cell membrane or internalization) in less than 5 min at 37 °C as well as 4 °C, suggesting some passive internalization processes. However, confocal microscopy experiments on live cells showed a punctuated intracellular

signal after 30 min of incubation with the Au NCs at 37 °C (Fig. 6), characteristic of an active uptake as endocytosis mediated internalization. Therefore, to explain the constant positive signal observed at 4 °C by flow cytometry, we assume Au NCs remain adsorbed on the cellular membrane. Interestingly, we also observed that almost all the cells are labeled as soon as 5 min after contact with AuSG-2Arg at 37 °C but that this percentage decreases rapidly with time and less than 50% of the cells are still positive after 45 min (Fig. 5A and S5†). If the AuSG-2Arg are internalized and found in intracellular vesicles, we could first hypothesize that this loss of PL intensity within the cells was related to their degradation in endosomes or lysosomes. However, this decrease of PL intensity does not appear to be related to the acidification of endosomes vesicles during their maturation toward lysosomes since AuSG-2Arg are stable for 48 h in PBS at pH 4 or 5 at room temperature. Numerous studies have shown the spontaneous biosynthesis of Au NCs inside cancer cells[34,35] or the displacement of initial organic thiol ligands from Au NPs[36] thanks to the intracellular SG but this is usually slower and necessitates several hours or days of contact. A loss of the PL intensity of the AuSG-2Arg due to their intramolecular remodeling in contact with the cytosolic glutathione, if the AuSG-2Arg passed spontaneously through the cell membrane to the cytoplasm, was thus unlikely to happen in our case, i.e. in less than 45 min. It is thus also possible that AuSG-2Arg are internalized, recycled rapidly and released in the extracellular medium within a few minutes. Seminal works reported the formation of nanopores by cationic NPs, crossing the cell membrane and inducing cell death.[9,10,12] Other studies revealed that small positively molecules[7,8] or negatively charged NPs with organized ligand shell[33] would be able to cross the cell membranes without transient poration. In our case, we observed low cytotoxic effects after the incubation of the cells with AuSG-2Arg or AuSG/SG-3Arg at various concentrations for 24 h (Fig. 7). We also found that the cells keep growing after their incubation for 24 h, 48 h or 72 h with these Au NCs at 250 µgAu mL^{-1} (Fig. S6†). This is an indirect evidence that these Au NCs are adsorbed and/or penetrated inside the cells without affecting their proliferative functions. Both the ultra-small size and the organized ligand shell of AuSG-2Arg and AuSG/SG-3Arg might be responsible of their capacity to interact with the cells without inducing toxicity. These Au NCs thus present particular intracellular trafficking properties and reduced toxicity that should be further investigated.

4. Conclusions

We use negatively charged (AuSG and AuSG-1Arg) and positively charged (AuSG-2Arg, AuSG/SG-3Arg and AuSG-3Arg) NCs with various amount of arginine moieties and investigated the influence of the global charge on the membrane interaction, the cell uptake and the toxicity.

We observed a clear difference of Au NCs-cells interaction depending on the amount of arginines on the Au NC surface. Flow cytometry measurements showed the absence of interaction with negatively charged NCs (AuSG and AuSG-1Arg) and fast interactions with positively charged NCs (AuSG-2Arg, AuSG/

SG-3Arg and AuSG-3Arg) in various conditions of medium, incubation time and temperature. Using artificial lipid layer model integrated in microfluidic device, we demonstrated a similar trend even at high serum content indicating the weak opsonization of highly positively charged Au NCs. This work highlights the importance of carefully controlling the surface functionalization of the Au NCs in terms of arginine multi-valency and density in order to achieve a high cellular uptake without inducing cytotoxicity.

Conflicts of interest

There are no conflicts to declare.

Acknowledgements

References

1 T. Vangijzegem, D. Stanicki and S. Laurent, *Expert Opin. Drug Delivery*, 2019, **16**, 69–78.
2 T. L. Doane and C. Burda, *Chem. Soc. Rev.*, 2012, **41**, 2885–2911.
3 S. Dufort, L. Sancey and J.-L. Coll, *Adv. Drug Delivery Rev.*, 2012, **64**, 179–189.
4 K. Murugan, Y. E. Choonara, P. Kumar, D. Bijukumar, L. C. du Toit and V. Pillay, *Int. J. Nanomed.*, 2015, **10**, 2191–2206.
5 I. Lynch and K. A. Dawson, *Nano Today*, 2008, **3**, 40–47.
6 P. d. Pino, B. Pelaz, Q. Zhang, P. Maffre, G. U. Nienhaus and W. J. Parak, *Mater. Horiz.*, 2014, **1**, 301–313.
7 E. Vives, J. P. Richard, C. Rispal and B. Lebleu, *Curr. Protein Pept. Sci.*, 2003, **4**, 125–132.
8 M. E. Herbig, F. Assi, M. Textor and H. P. Merkle, *Biochemistry*, 2006, **45**, 3598–3609.
9 C. M. Goodman, C. D. McCusker, T. Yilmaz and V. M. Rotello, *Bioconjugate Chem.*, 2004, **15**, 897–900.
10 J. Lovrić, H. S. Bazzi, Y. Cuie, G. R. A. Fortin, F. M. Winnik and D. Maysinger, *J. Mol. Med.*, 2005, **83**, 377–385.
11 J. Lin, H. Zhang, Z. Chen and Y. Zheng, *ACS Nano*, 2010, **4**, 5421–5429.
12 E. Fröhlich, *Int. J. Nanomed.*, 2012, **7**, 5577–5591.
13 A. M. Alkilany, P. K. Nagaria, C. R. Hexel, T. J. Shaw, C. J. Murphy and M. D. Wyatt, *Small*, 2009, **5**, 701–708.
14 Y. Guo, E. Terazzi, R. Seemann, J. B. Fleury and V. A. Baulin, *Sci. Adv.*, 2016, **2**, e1600261.
15 R. Jin, C. Zeng, M. Zhou and Y. Chen, *Chem. Rev.*, 2016, **116**, 10346–10413.
16 R. A. Murray, A. Escobar, N. G. Bastús, P. Andreozzi, V. Puntes and S. E. Moya, *NanoImpact*, 2018, **9**, 102–113.
17 E. Porret, L. Sancey, A. Martín-Serrano, M. I. Montañez, R. Seeman, A. Yahia-Ammar, H. Okuno, F. Gomez, A. Ariza, N. Hildebrandt, J.-B. Fleury, J.-L. Coll and X. Le Guével, *Chem. Mater.*, 2017, **29**, 7497–7506.
18 S. Gao, D. Chen, Q. Li, J. Ye, H. Jiang, C. Amatore and X. Wang, *Sci. Rep.*, 2014, **4**, 4384.
19 Y. Negishi, K. Nobusada and T. Tsukuda, *J. Am. Chem. Soc.*, 2005, **127**, 5261–5270.
20 Y. Negishi, Y. Takasugi, S. Sato, H. Yao, K. Kimura and T. Tsukuda, *J. Am. Chem. Soc.*, 2004, **126**, 6518–6519.
21 R. D. Vinluan, J. Liu, C. Zhou, M. Yu, S. Yang, A. Kumar, S. Sun, A. Dean, X. Sun and J. Zheng, *ACS Appl. Mater. Interfaces*, 2014, **6**, 11829–11833.
22 M. Yu, C. Zhou, J. Liu, J. D. Hankins and J. Zheng, *J. Am. Chem. Soc.*, 2011, **133**, 11014–11017.
23 L. Zhang and E. Wang, *Nano Today*, 2014, **9**, 132–157.
24 X. Liu, C. Liu, J. Zhou, C. Chen, F. Qu, J. J. Rossi, P. Rocchi and L. Peng, *Nanoscale*, 2015, **7**, 3867–3875.
25 E. Porret, M. Jourdan, B. Gennaro, C. Comby-Zerbino, F. Bertorelle, V. Trouillet, X. Qiu, C. Zoukimian, D. Boturyn, N. Hildebrandt, R. Antoine, J.-L. Coll and X. Le Guével, *J. Phys. Chem. C*, 2019, **123**, 26705–26717.
26 Y. Guo, M. Werner, J. B. Fleury and V. A. Baulin, *Phys. Rev. Lett.*, 2020, **124**, 038001.
27 J. Friend and L. Yeo, *Biomicrofluidics*, 2010, **4**, 026502.
28 B. Gray, *Biochem. Educ.*, 1981, **9**, 111.
29 H. Bayley, B. Cronin, A. Heron, M. A. Holden, W. L. Hwang, R. Syeda, J. Thompson and M. Wallace, *Mol. BioSyst.*, 2008, **4**, 1191–1208.
30 F. de Chaumont, S. Dallongeville, N. Chenouard, N. Hervé, S. Pop, T. Provoost, V. Meas-Yedid, P. Pankajakshan, T. Lecomte, Y. Le Montagner, T. Lagache, A. Dufour and J.-C. Olivo-Marin, *Nat. Methods*, 2012, **9**, 690–696.
31 N. Fricke and R. Dimova, *Biophys. J.*, 2016, **111**, 1935–1945.
32 R. Dasgupta, M. S. Miettinen, N. Fricke, R. Lipowsky and R. Dimova, *Proc. Natl. Acad. Sci. U. S. A.*, 2018, **115**, 5756–5761.
33 A. Verma, O. Uzun, Y. Hu, Y. Hu, H.-S. Han, N. Watson, S. Chen, D. J. Irvine and F. Stellacci, *Nat. Mater.*, 2008, **7**, 588–595.
34 J. Wang, J. Ye, H. Jiang, S. Gao, W. Ge, Y. Chen, C. Liu, C. Amatore and X. Wang, *RSC Adv.*, 2014, **4**, 37790–37795.
35 J. Wang, G. Zhang, Q. Li, H. Jiang, C. Liu, C. Amatore and X. Wang, *Sci. Rep.*, 2013, **3**, 1157.
36 R. Hong, G. Han, J. M. Fernández, B.-j. Kim, N. S. Forbes and V. M. Rotello, *J. Am. Chem. Soc.*, 2006, **128**, 1078–1079.